Fig s1

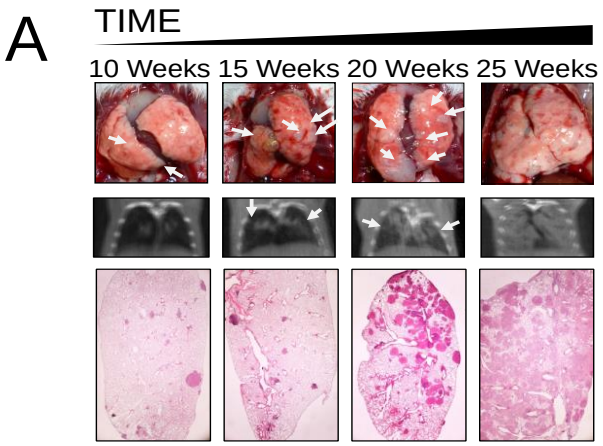
A
TIME
10 Weeks
15 Weeks
20 Weeks
25 Weeks

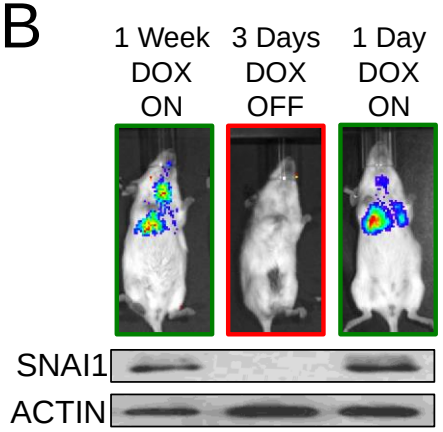
B
1 Week DOX ON
3 Days DOX OFF
1 Day DOX ON
SNAI1
ACTIN

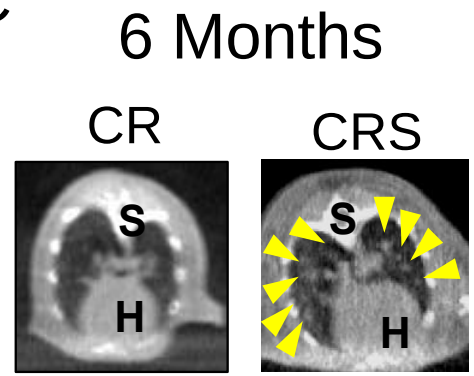
C
6 Months
CR
CRS
S
H

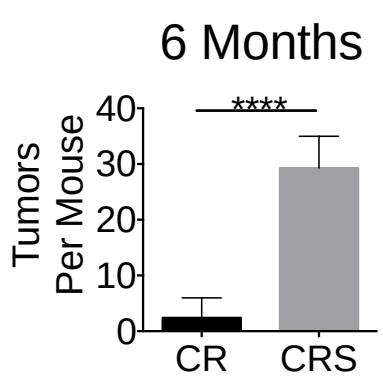
D
6 Months
Tumors Per Mouse
****
CR
CRS

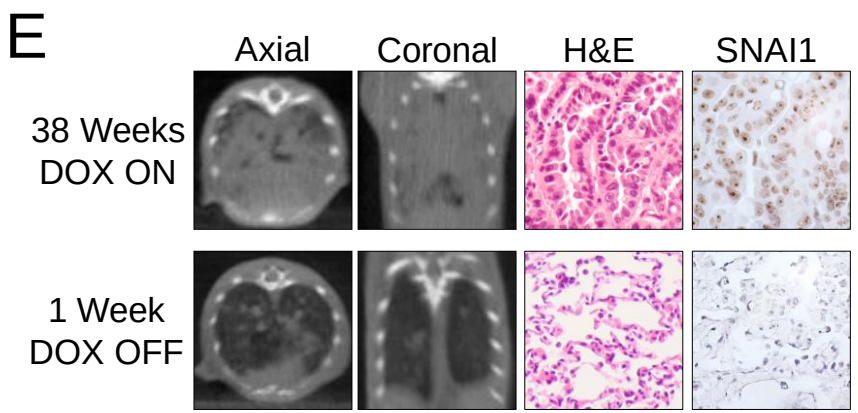
E
Axial
Coronal
H&E
SNAI1
38 Weeks DOX ON
1 Week DOX OFF

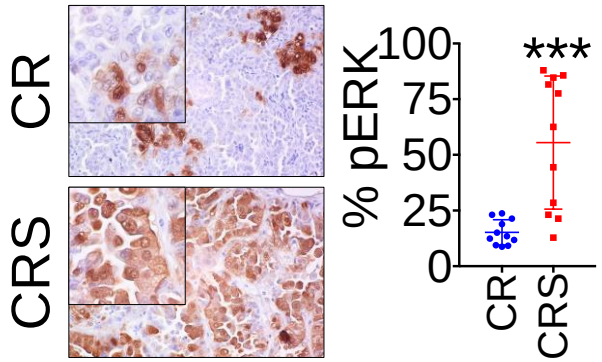
F
CR
CRS
% pERK
***
CR
CRS

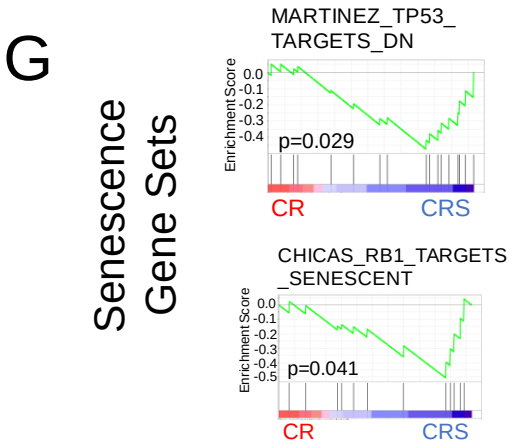
G
Senescence Gene Sets
MARTINEZ_TP53_TARGETS_DN
p=0.029
CR
CRS
CHICAS_RB1_TARGETS_SENESCENT
p=0.041
CR
CRS

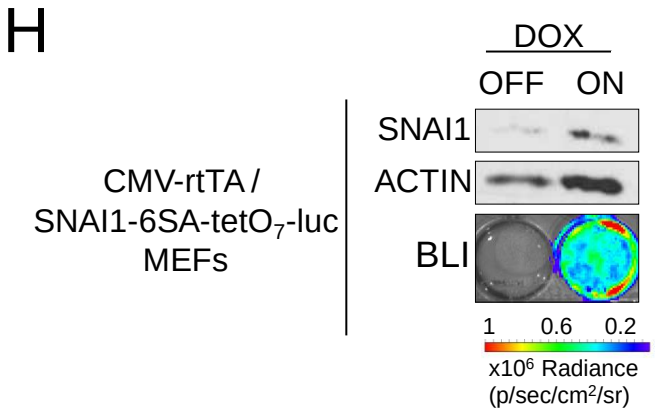
H
CMV-rtTA / SNAI1-6SA-tetO7-luc MEFs
DOX
OFF
ON
SNAI1
ACTIN
BLI
1
0.6
0.2
x10⁶ Radiance (p/sec/cm²/sr)

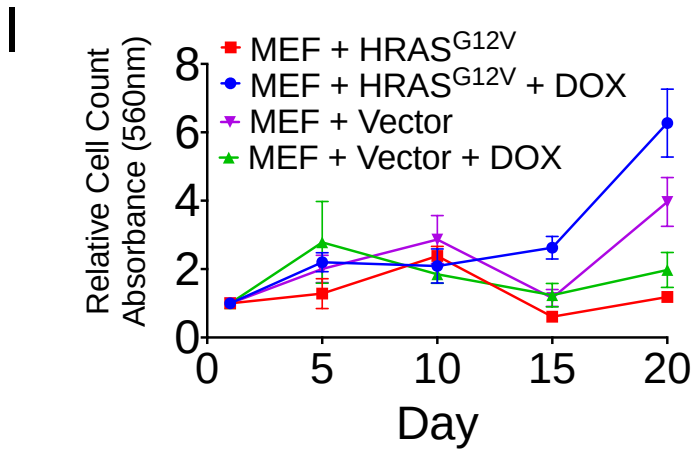
I
MEF + HRASG12V
MEF + HRASG12V + DOX
MEF + Vector
MEF + Vector + DOX
Relative Cell Count Absorbance (560nm)
Day

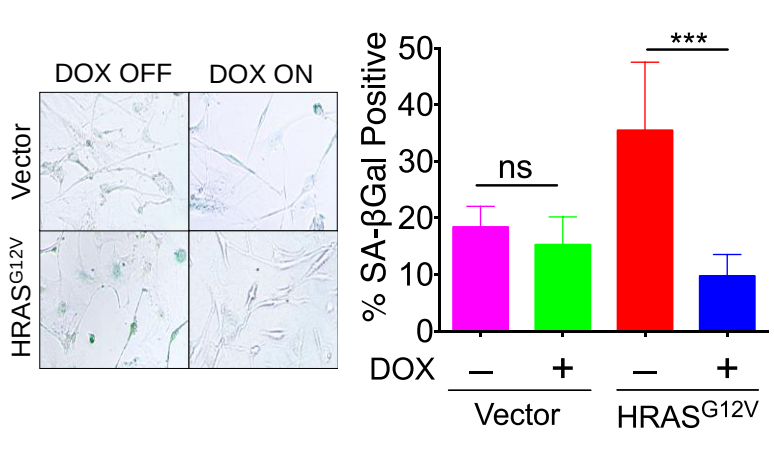
J
DOX OFF
DOX ON
Vector
HRASG12V
% SA-βGal Positive
***
ns
DOX
Vector
HRASG12V

Fig. s1. Characterizing a Kras^{G12D} driven EMT mouse model of NSCLC. A, 25 week time course of CRS mouse model with inducible SNAI1 expression monitored by gross anatomy, cone-beam computed tomography (CBCT) scans, and hematoxylin and eosin (H&E) staining. **B**, Doxycycline (DOX) inducible expression of SNAI1 was verified with bioluminescence imaging (BLI) and SNAI Western blotting. **C, D,** CR and CRS mouse tumor CBCT scans (**C**) and quantification (**D**) at 6 months. **E,** Tumor regression of CRS mice 38 weeks post-removal of DOX from mice drinking water as seen by CBCT, H&E, and SNAI1 immunohistochemistry (IHC) staining. **F,** IHC staining of phosphorylated ERK (pERK) IHC in CRS mouse tumors compared to CR mouse tumors. **G,** Gene Set Enrichment Analysis (GSEA) enrichment plots (data sets obtained from the Molecular Signatures Database) were generated using differentially expressed genes between CR and CRS mice and identified significantly matching gene sets involving senescence. **H-J,** Inducible SNAI1 expressing MEFs overcome HRAS^{G12D} induced OIS. Validation of the DOX inducible SNAI1 expressing MEFs by Western blotting and luciferase reporter (visualized by BLI, **H**). **I,J,** Inducible SNAI1 MEFs were transduced with HRAS^{G12V} or vector control with or without SNAI1 expression ($\pm$ 2μg/mL DOX in cell culture media) and relative change in cell number (**I**; P<0.001 by two-way ANOVA followed by Holm-Sidak's multiple comparisons test), SA-βGal staining (**J**) were measured. Error bars, mean $\pm$ standard deviation (s.d.). P values were derived from an unpaired, two-tailed Student's t-test (*P<0.05; ***P<0.001; ****P<0.0001).

Fig s2

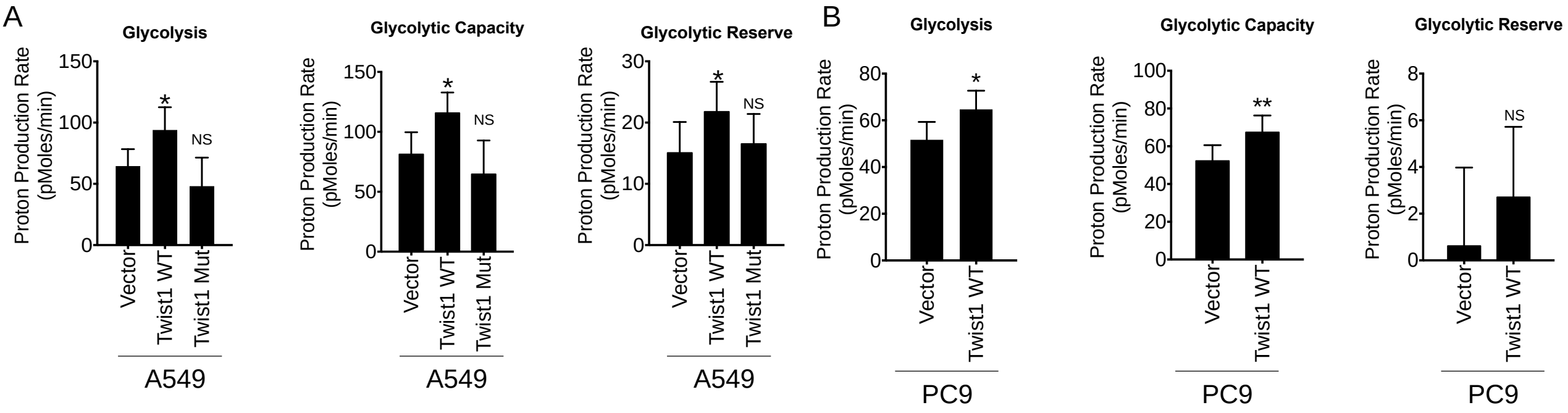
A
Glycolysis
Glycolytic Capacity
Glycolytic Reserve
Proton Production Rate (pMoles/min)
Vector
Twist1 WT
Twist1 Mut
NS
A549
B
PC9

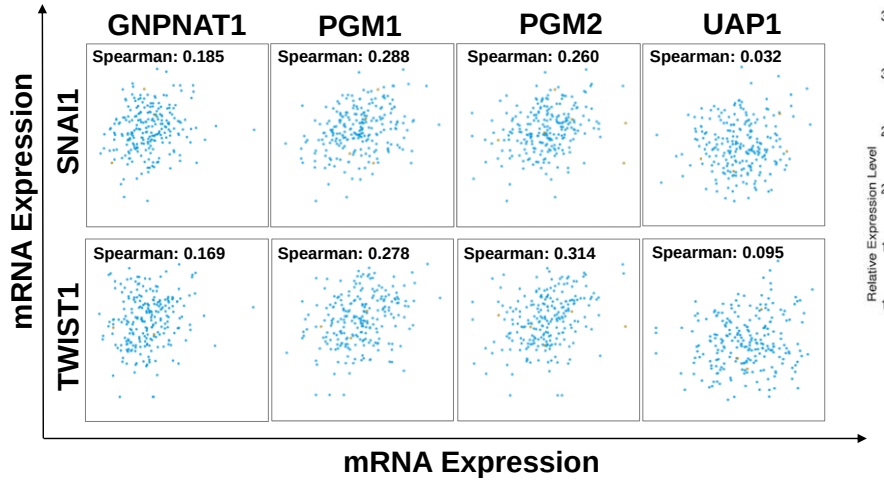
C
GNPNAT1
PGM1
PGM2
UAP1
SNAI1
TWIST1
Spearman: 0.185
Spearman: 0.288
Spearman: 0.260
Spearman: 0.032
Spearman: 0.169
Spearman: 0.278
Spearman: 0.314
Spearman: 0.095
mRNA Expression

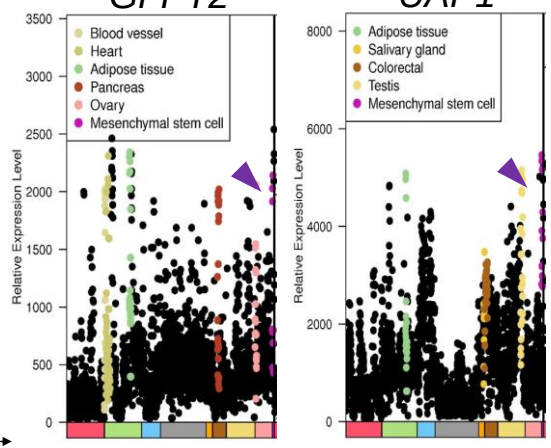
D
GFPT2
UAP1
Blood vessel
Heart
Adipose tissue
Pancreas
Ovary
Mesenchymal stem cell
Adipose tissue
Salivary gland
Colorectal
Testis
Mesenchymal stem cell
Relative Expression Level

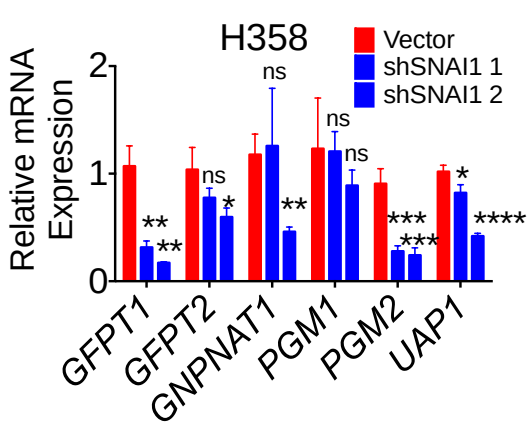
E
H358
Vector
shSNAI1 1
shSNAI1 2
Relative mRNA Expression
GFPT1
GFPT2
GNPNAT1
PGM1
PGM2
UAP1

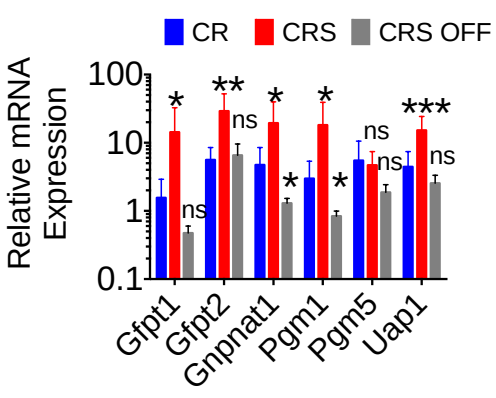
F
CR
CRS
CRS OFF
Relative mRNA Expression
Gfpt1
Gfpt2
Gnpnat1
Pgm1
Pgm5
Uap1

Fig. s2. The EMT increase glycolysis and induce the HBP gene expression in human NSCLC. A, B, Seahorse analysis of glycolytic flux of EMT NSCLC cells. Glycolytic activity, capacity, and reserve was determined in real-time using the Seahorse extracellular flux analyzer for vector, Twist1, and loss of function Twist1 in A549 (**A**) and PC9 (**B**) cells. **C,** Human tissue gene expression from Medisapiens In Silico Transcriptomics (IST) from 60 healthy tissues; significant gene expression of GFPT2 and UAP1 were found in mesenchymal stem cells (purple arrows). **D, E,** mRNA expression of the HBP genes by qPCR in vitro with knocking down Snai1 in NSCLC cell lines H358 (**D**), and in vivo autochthonous lung tumor mouse models with and without DOX inducible expression of SNAI1/KrasG12D (**E**). Error bars, mean ± s.d. P values were derived from an unpaired, two-tailed Student’s t-test. (ns $P \geq 0.05$; *$P < 0.05$; **$P < 0.01$).

Fig s3

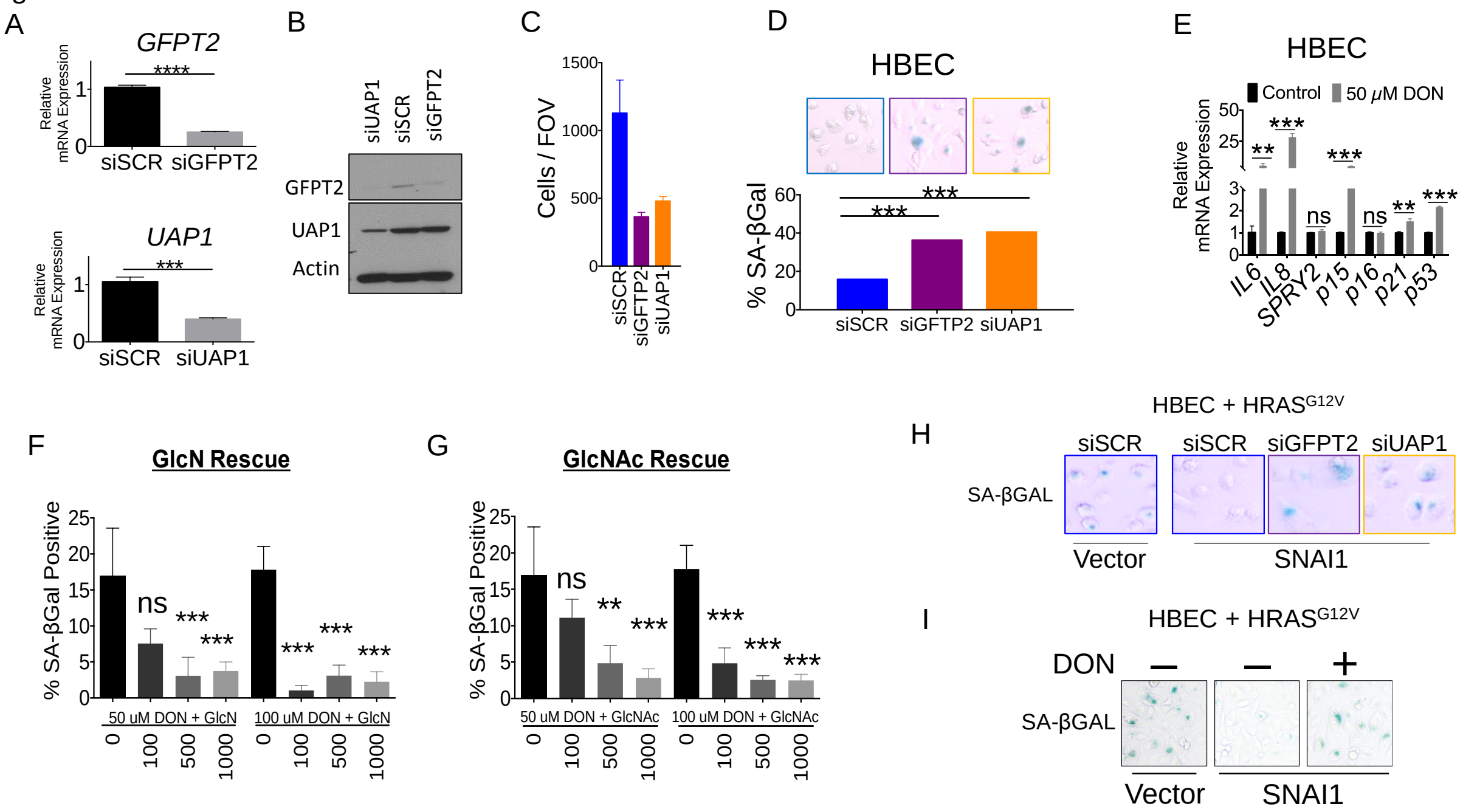
A
GFPT2
Relative mRNA Expression
****
siSCR siGFPT2
UAP1
***
siSCR siUAP1
B
siUAP1 siSCR siGFPT2
GFPT2
UAP1
Actin
C
Cells / FOV
siSCR siGFTP2 siUAP1
D
HBEC
% SA-βGal
siSCR siGFTP2 siUAP1
E
HBEC
Control 50 μM DON
Relative mRNA Expression
IL6 IL8 SPRY2 p15 p16 p21 p53
F
GlcN Rescue
% SA-βGal Positive
50 uM DON + GlcN
100 uM DON + GlcN
G
GlcNAc Rescue
50 uM DON + GlcNAc
100 uM DON + GlcNAc
H
HBEC + HRASG12V
siSCR siSCR siGFPT2 siUAP1
SA-βGAL
Vector SNAI1
I
HBEC + HRASG12V
DON
SA-βGAL
Vector SNAI1

Fig. s3. The HBP is critical for senescence of normal lung cells. A-D, Genetic inhibition of the HBP with knockdown of *GFPT2* and *UAP1* as shown by mRNA (**A**) and protein levels (**B**) and resulting cell number change per field of view (FOV; **C**) and SA-βGal staining (**D**) (statistical analysis by One-way ANOVA with Dunnett's multiple comparison test). **E-G,** qPCR of senescence gene expression in HBECs treated with high concentration (50 μM) of DON for 48 hours (**E**) and metabolic rescue by supplementation with glucosamine (GlcN; **F**) or N-acetylglucosamine (GlcNAc; **G**) (statistical analysis by One-way ANOVA with Dunnett's multiple comparison test). **H, I**, Bright field images of SA-βGal staining using genetic siRNA (**H**) and pharmacological DON (**I**) inhibition of the HBP.

Fig s4

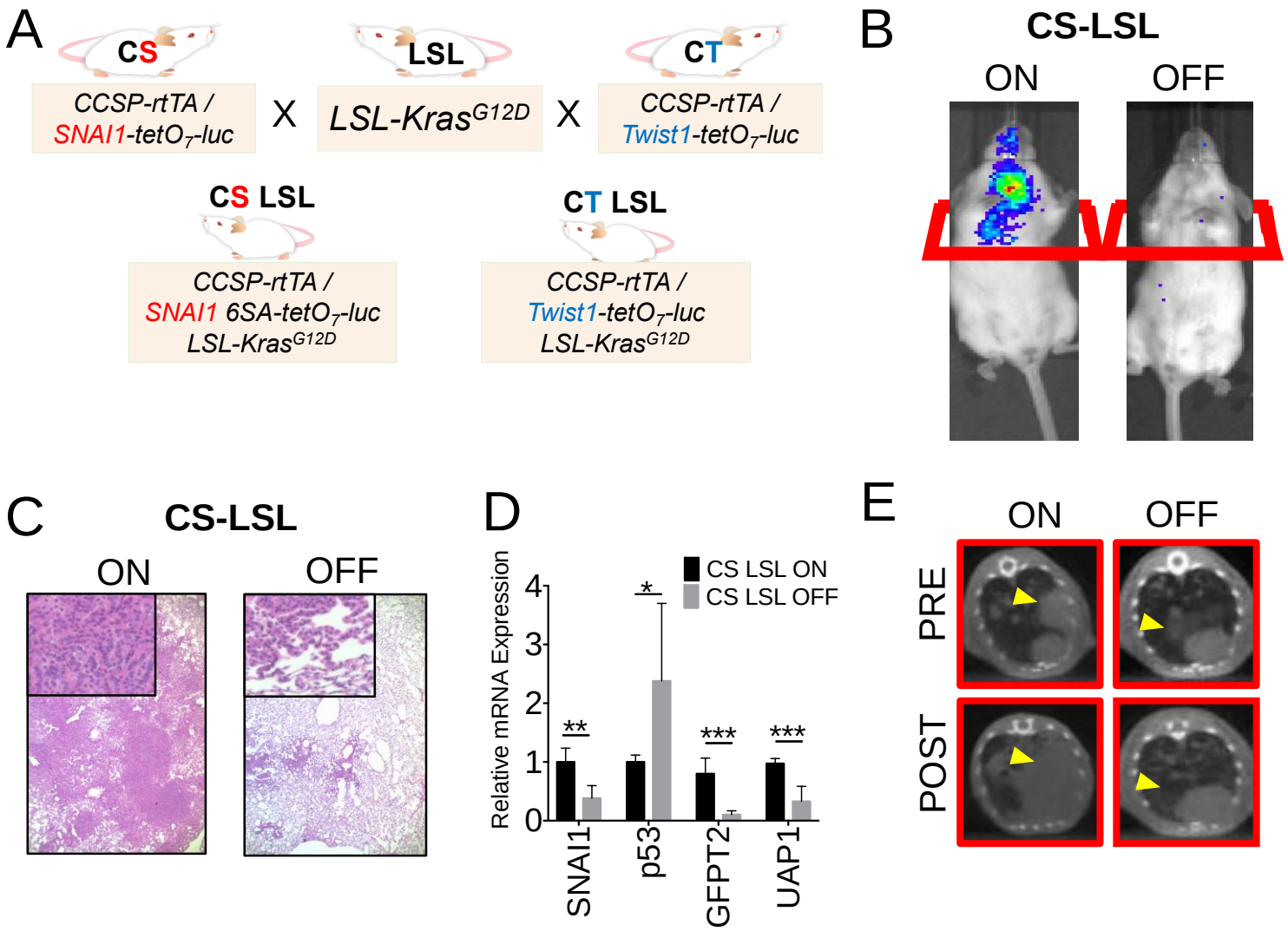
A
CS
CCSP-rtTA /
SNAI1-tetO7-luc
X
LSL
LSL-KrasG12D
X
CT
CCSP-rtTA /
Twist1-tetO7-luc
CS LSL
CCSP-rtTA /
SNAI1 6SA-tetO7-luc
LSL-KrasG12D
CT LSL
CCSP-rtTA /
Twist1-tetO7-luc
LSL-KrasG12D
B
CS-LSL
ON
OFF
C
CS-LSL
ON
OFF
D
Relative mRNA Expression
CS LSL ON
CS LSL OFF
SNAI1
p53
GFPT2
UAP1
E
ON
OFF
PRE
POST

Fig. s4. Characterizing a novel Kras^{G12D} driven EMT mouse model of NSCLC. A, Breeding schematic of the *Lox-Stop-Lox Kras^{G12D}* (LSL) model with DOX inducible lung specific expressing *SNAI1* (CS) and *Twist1* (CT) mouse models to generate DOX inducible EMT models with conditional expression of *Kras^{G12D}* upon intranasal administration of Ad-CMV-iCre (AdCre) virus. ON and OFF indicate animals with or without DOX, respectively in their drinking water. **B-E**, Representative BLI (**B**), H&E (**C**), qPCR (**D**) and CT (**E**), of CS-LSL mice with and without inactivation of SNAI1 expression by withdrawing DOX from mouse drinking water, while maintaining expression of *Kras^{G12D}* expression. (**E**) PRE and POST represents CT scans obtained prior to and after DOX withdrawal, respectively. Unless stated, error bars, mean ± s.d. P values were derived from an unpaired, two-tailed Student's t-test (***P<0.001; ****P<0.0001).

Fig s5

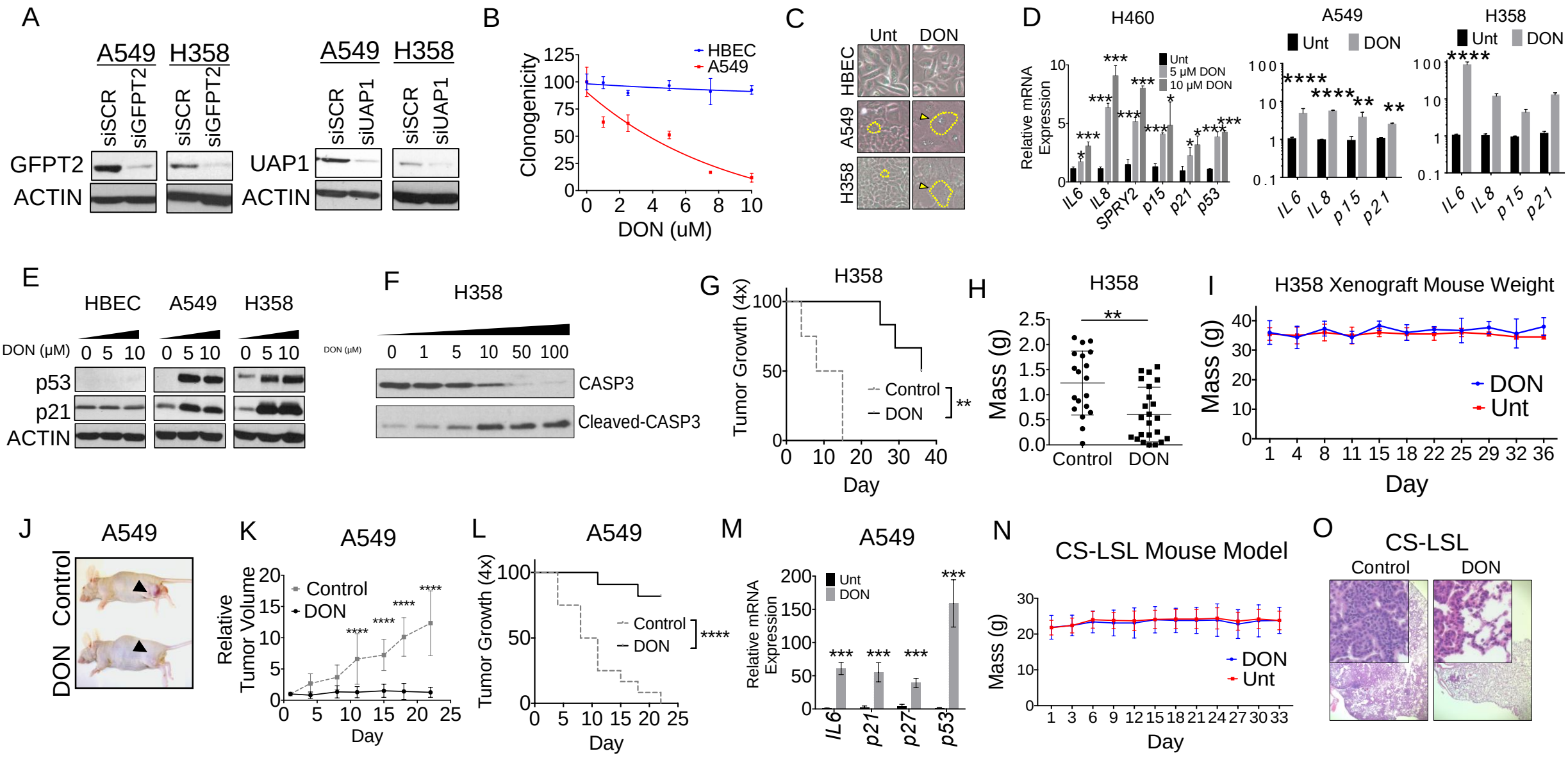
A
A549
H358
siSCR
siGFPT2
siUAP1
GFPT2
UAP1
ACTIN
B
Clonogenicity
HBEC
A549
DON (uM)
C
Unt
DON
HBEC
A549
H358
D
H460
A549
H358
Unt
5 μM DON
10 μM DON
Relative mRNA Expression
IL6
IL8
SPRY2
p15
p21
p53
E
HBEC
A549
H358
DON (μM)
p53
p21
ACTIN
F
H358
CASP3
Cleaved-CASP3
G
H358
Tumor Growth (4x)
Control
DON
Day
H
H358
Mass (g)
Control
DON
I
H358 Xenograft Mouse Weight
Mass (g)
DON
Unt
Day
J
A549
Control
DON
K
A549
Relative Tumor Volume
Control
DON
Day
L
A549
Tumor Growth (4x)
Control
DON
Day
M
A549
Relative mRNA Expression
Unt
DON
IL6
p21
p27
p53
N
CS-LSL Mouse Model
Mass (g)
DON
Unt
Day
O
CS-LSL
Control
DON

Fig. s5. Inhibition of the HBP reduces cell viability and abrogates tumor growth and promotes senescence phenotypes. A, Genetic knockdown in A549 and H358 cells with siRNA targeting *GFPT2* and *UAP1* confirmed on the protein level by Western blot. **B,** Clonogenicity measured by crystal violet stained colonies on 10 cm dishes of A549 cells after 48 hours of pharmacological inhibition of the HBP with DON treatment. **C,** Senescence morphology. **D-F**, qPCR (**D**) Western blot (**E, F**) for markers of senescence and apoptosis (cleaved caspase 3) in 3 NSCLC cell lines upon 48 hour treatment of DON. The actin blot in (**E**) was from a parallel, contemporaneously run blot. **G-I,** H358 NSCLC cells ($8x10^6$) were injected into ~5 week old athymic nude female mice. Within the first week (visible tumors of ~50 mm3), mice were treated with 20 mg/kg/week DON and were assessed for tumor growth ($P<0.01$ by long-rank test; **G**), tumor mass (**H**), and with no noticeable toxicities to the mice measured by body mass (**I**) ($P>0.05$ by Two-way ANOVA) over a 5 week period. **J-M**, Likewise, A549 NSCLC cells ($1x10^6$) were implanted and treated with 20 mg/kg/week DON and were assessed for tumor size (**J**), tumor volume (n≥12 tumors per arm; $P<0.0001$ by two-way ANOVA followed by Holm-Sidak's multiple comparisons test; (**K)**, tumor growth ($P<0.0001$ by log-rank test; **L**), and markers of senescence (**M**) over a 3 week period. **N**, CS-LSL mouse mass with and without DON treatment over 4 weeks ($P>0.05$ by Two-way ANOVA). and H&E staining (**O**) at 5 weeks post-AdCre.Unless stated. Error bars, mean ± s.d. P values were derived from an unpaired, two-tailed Student's t-test (*$P<0.05$; ***$P<0.001$).

Fig s6

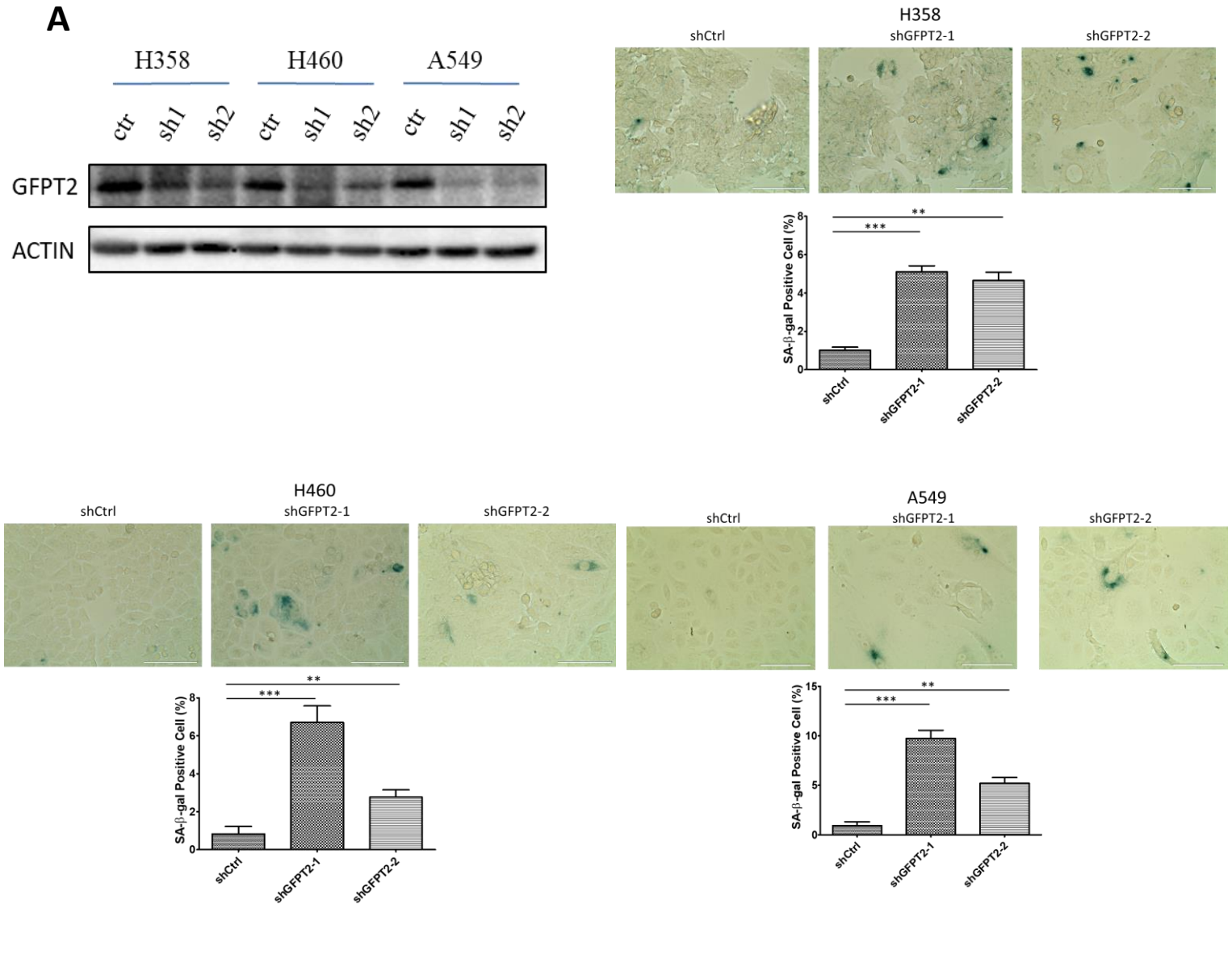
A
H358
H460
A549
ctr
sh1
sh2
GFPT2
ACTIN
H358
shCtrl
shGFPT2-1
shGFPT2-2
SA-β-gal Positive Cell (%)
H460
A549
B
C
Relative colony formation ability
p=0.100
p=0.001
p=0.963
p<0.001
p=0.013
p=0.004
p=0.001
GFPT2

Fig. S6. Inhibiting HBP by *GFPT2* knockdown resulted in more senescent cells and decreased clonogenic ability of lung cancer cells. A, SA-β-Gal staining of lung cancer cell lines after *GFPT2* knockdown (**p<0.001, ***p<0.0001). **B-C**, Clonogenic assays of lung cancer cell lines with *GFPT2* (**B**) knockdown or (**C**) GFPT2 overexpression.

Fig s7

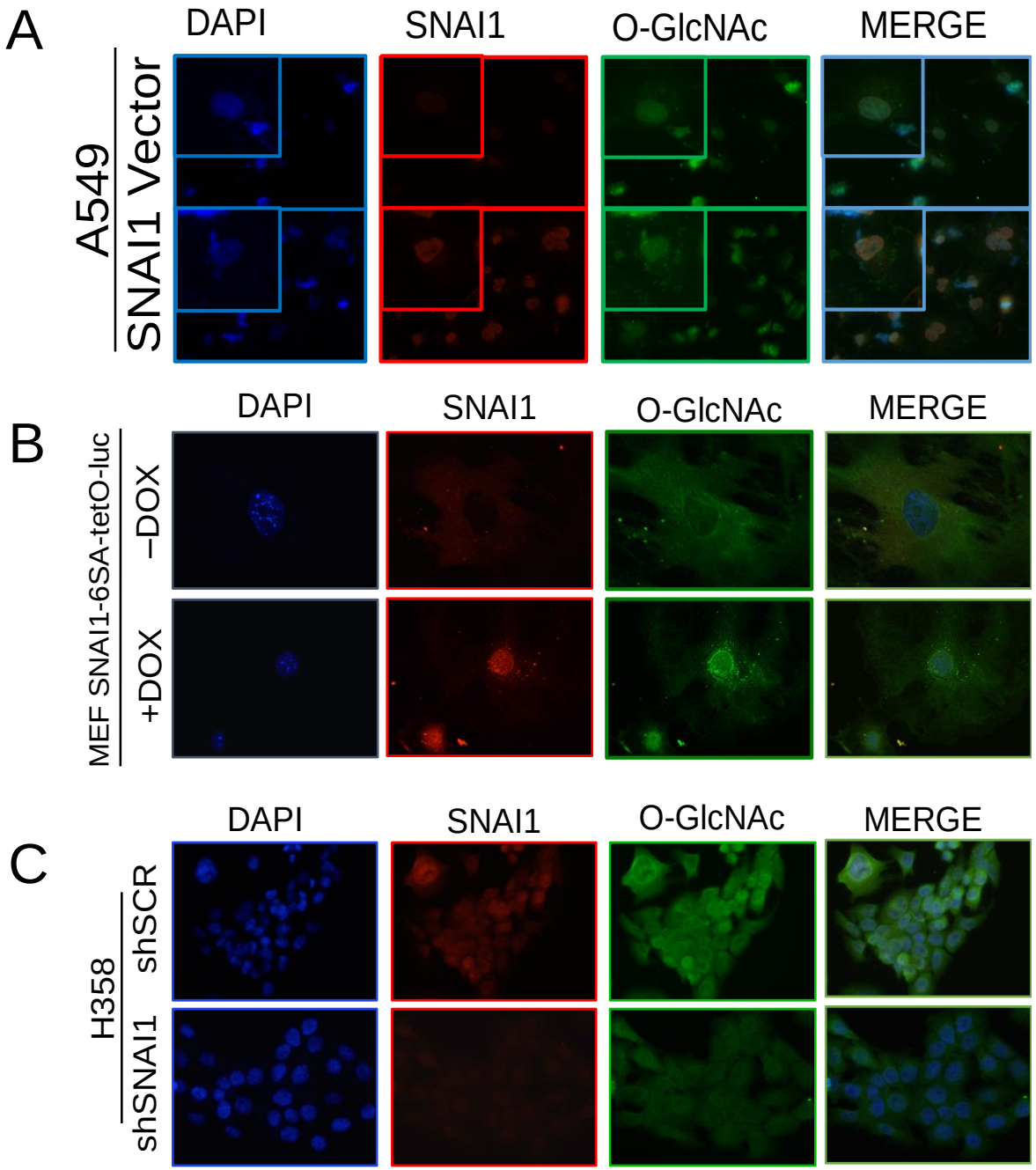
A
DAPI
SNAI1
O-GlcNAc
MERGE
A549
SNAI1 Vector
B
DAPI
SNAI1
O-GlcNAc
MERGE
MEF SNAI1-6SA-tetO-luc
–DOX
+DOX
C
DAPI
SNAI1
O-GlcNAc
MERGE
H358
shSCR
shSNAI1

Fig. s7. SNAI1 expression correlates with O-GlcNAcylation. A-C, Immununofluoresence (IF) of SNAI1 and O-GlcNAc co-expressing A549 NSCLC cells (with elevated O-GlcNAc cytoplasmic immunopositive foci) (**A**), 48 hour DOX inducible SNAI1 expressing MEFs (**B**), and stable knockdown of *SNAI1* in H358 NSCLC cells (**C**) (blue – DAPI; red – SNAI1; green – O-GlcNAc [RL2]).

Fig s8

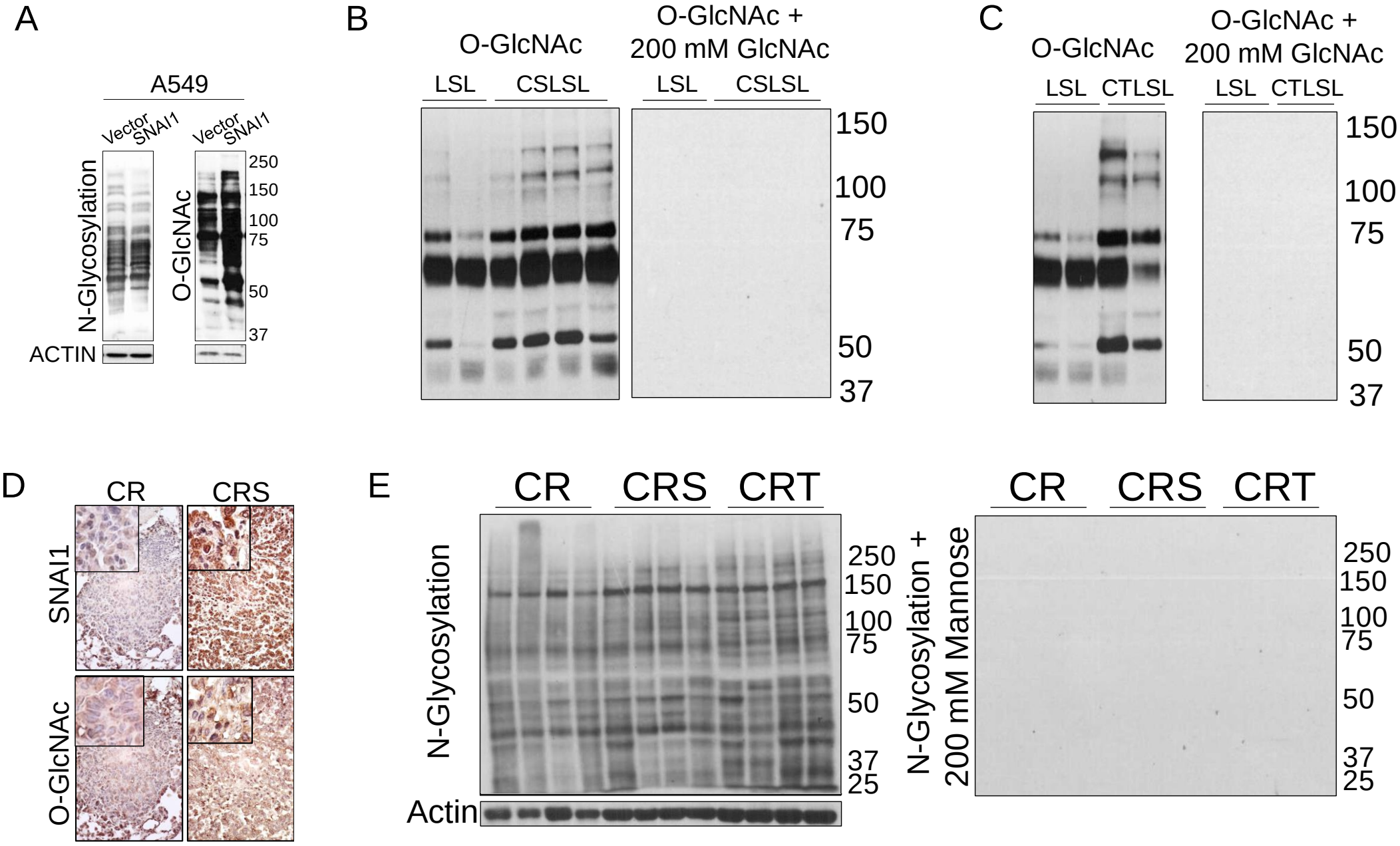
A
A549
Vector
SNAI1
Vector
SNAI1
N-Glycosylation
O-GlcNAc
ACTIN
250
150
100
75
50
37
B
O-GlcNAc
O-GlcNAc +
200 mM GlcNAc
LSL
CSLSL
LSL
CSLSL
150
100
75
50
37
C
O-GlcNAc
O-GlcNAc +
200 mM GlcNAc
LSL
CTLSL
LSL
CTLSL
150
100
75
50
37
D
CR
CRS
SNAI1
O-GlcNAc
E
CR
CRS
CRT
N-Glycosylation
Actin
250
150
100
75
50
37
25
CR
CRS
CRT
N-Glycosylation +
200 mM Mannose
250
150
100
75
50
37
25

Fig. s8. N-Linked glycosylation and O-GlcNAcylation in lung cancer cell line and novel EMT mouse models of lung cancer. A, Effects on total N-glycosylation and O-GlcNAcylation with 48 hour SNAI1 transient expression in A549 cells. **B-D,** LSL mouse tumors were compared to CS-LSL (**B**) and CT-LSL (**C**) mouse tumors for O-GlcNAcylation by Western blot. **(D)** IHC staining of O-GlcNAc and Snai1 on CR, CRS mouse tumors. **E,** CR, CRS, and CRT mouse tumors were assessed for N-glycosylation with the terminal glycosyl/mannosyl binding lectin (concanavalin A [conA]) and specificity of the conA lectin was assessed by blotting with 200 mM Mannose

Fig s9

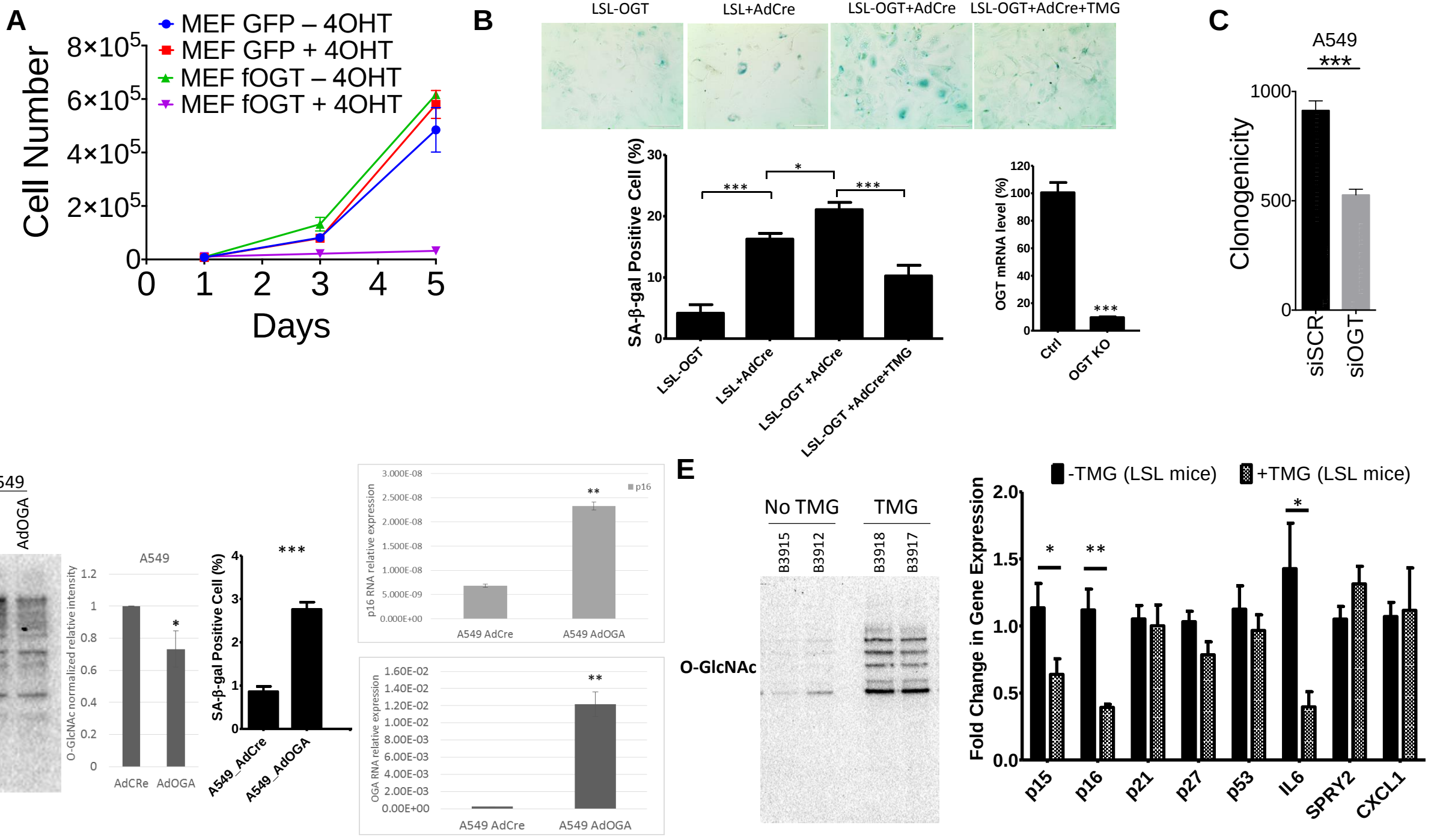
A
MEF GFP – 4OHT
MEF GFP + 4OHT
MEF fOGT – 4OHT
MEF fOGT + 4OHT
Cell Number
8×10^5
6×10^5
4×10^5
2×10^5
0
0 1 2 3 4 5
Days
B
LSL-OGT
LSL+AdCre
LSL-OGT+AdCre
LSL-OGT+AdCre+TMG
SA-β-gal Positive Cell (%)
30
20
10
0
***
*
***
LSL-OGT
LSL+AdCre
LSL-OGT +AdCre
LSL-OGT +AdCre+TMG
OGT mRNA level (%)
120
100
80
60
40
20
0
***
Ctrl
OGT KO
C
A549
***
Clonogenicity
1000
500
0
siSCR
siOGT
D
A549
AdCre
AdOGA
O-GlcNAc normalized relative intensity
1.2
1
0.8
0.6
0.4
0.2
0
A549
*
AdCRe
AdOGA
SA-β-gal Positive Cell (%)
4
3
2
1
0
***
A549_AdCre
A549_AdOGA
p16 RNA relative expression
3.000E-08
2.500E-08
2.000E-08
1.500E-08
1.000E-08
5.000E-09
0.000E+00
p16
**
A549 AdCre
A549 AdOGA
OGA RNA relative expression
1.60E-02
1.40E-02
1.20E-02
1.00E-02
8.00E-03
6.00E-03
4.00E-03
2.00E-03
0.00E+00
**
A549 AdCre
A549 AdOGA
E
No TMG
TMG
B3915
B3912
B3918
B3917
O-GlcNAc
-TMG (LSL mice)
+TMG (LSL mice)
Fold Change in Gene Expression
2.0
1.5
1.0
0.5
0.0
*
**
*
p15
p16
p21
p27
p53
IL6
SPRY2
CXCL1

Fig. s9. OGT and cell viability. A, Cell proliferation of MEF cells with inducible OGT knockout by tamoxifen (4-OHT) ($p<0.0001$ by Two-way ANOVA). **B,** SA-beta-Galactosidase staining 8 days after AdCre treatment on primary type II pneumocytes isolated from LSL-$Kras^{G12D}$ (LSL) and LSL-$Kras^{G12D}/OGT^{fl/Y}$ (LSL-OGT) mice, with or without OGA inhibitor (Thiamet-G (TMG), 50uM) treatment (*$p<0.01$, ***$p<0.0001$). **C,** Clonogenic assay of A549 cells with *Ogt* knockdown by siRNA ($p<0.0001$ by t test). **D,** Overexpression of *OGA* in A549 cell line lead to cellular senescence. Western-blot and quantification of total O-GlcNAc (left two panels), (AdCre vs AdOGA, n=3, t-test $p=0.014$), quantification of SA-β-Gal staining after OGA overexpression (*** $p<0.0001$) and RT-PCR for *p16* and *OGA* (** $p<0.001$). **E,** TMG treatment resulted in elevated protein O-GlcNAcylation and decreased expression level of several genes associated with senescence in the lung tissue of LSL-$Kras^{G12D}$ mice (LSL) (*$p<0.01$, **$p<0.001$).

Fig s10

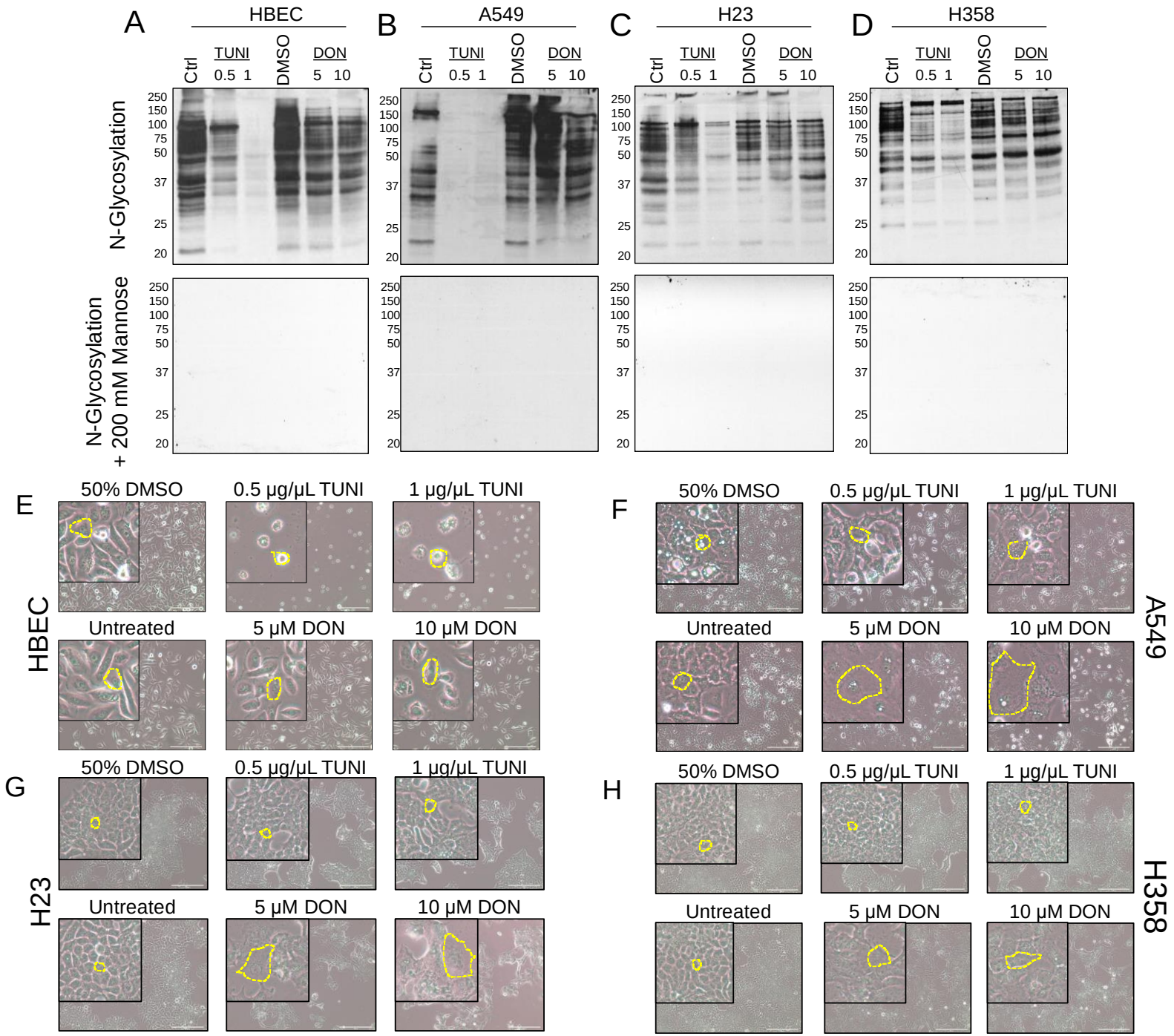
A
HBEC
B
A549
C
H23
D
H358
Ctrl
TUNI
0.5 1
DMSO
DON
5 10
N-Glycosylation
N-Glycosylation
+ 200 mM Mannose
250
150
100
75
50
37
25
20
E
F
G
H
50% DMSO
0.5 µg/µL TUNI
1 µg/µL TUNI
Untreated
5 µM DON
10 µM DON
HBEC
A549
H23
H358

Fig. s10. Inhibition of N-glycosylation with tunicamycin does not induce senescent phenotypes, unlike inhibition of the HBP with DON. A-E, Normal (**A**) and NSCLC cells (**B-D**) were treated with either tunicamycin (TUNI, 0.5 or 1 µg/µL) or DON (5 or 10 µM) and blotted with concanavalin A (ConA) to assess N-link glycosylation occupancy; ConA was assessed for specificity by competitive blotting with 200 mM mannose. **E-H**, Senescent morphology was seen in DON (5 or 10 µM) treated NSCLC cells, but not with TUNI treatment (0.5 or 1 µg/µL).

Fig s11

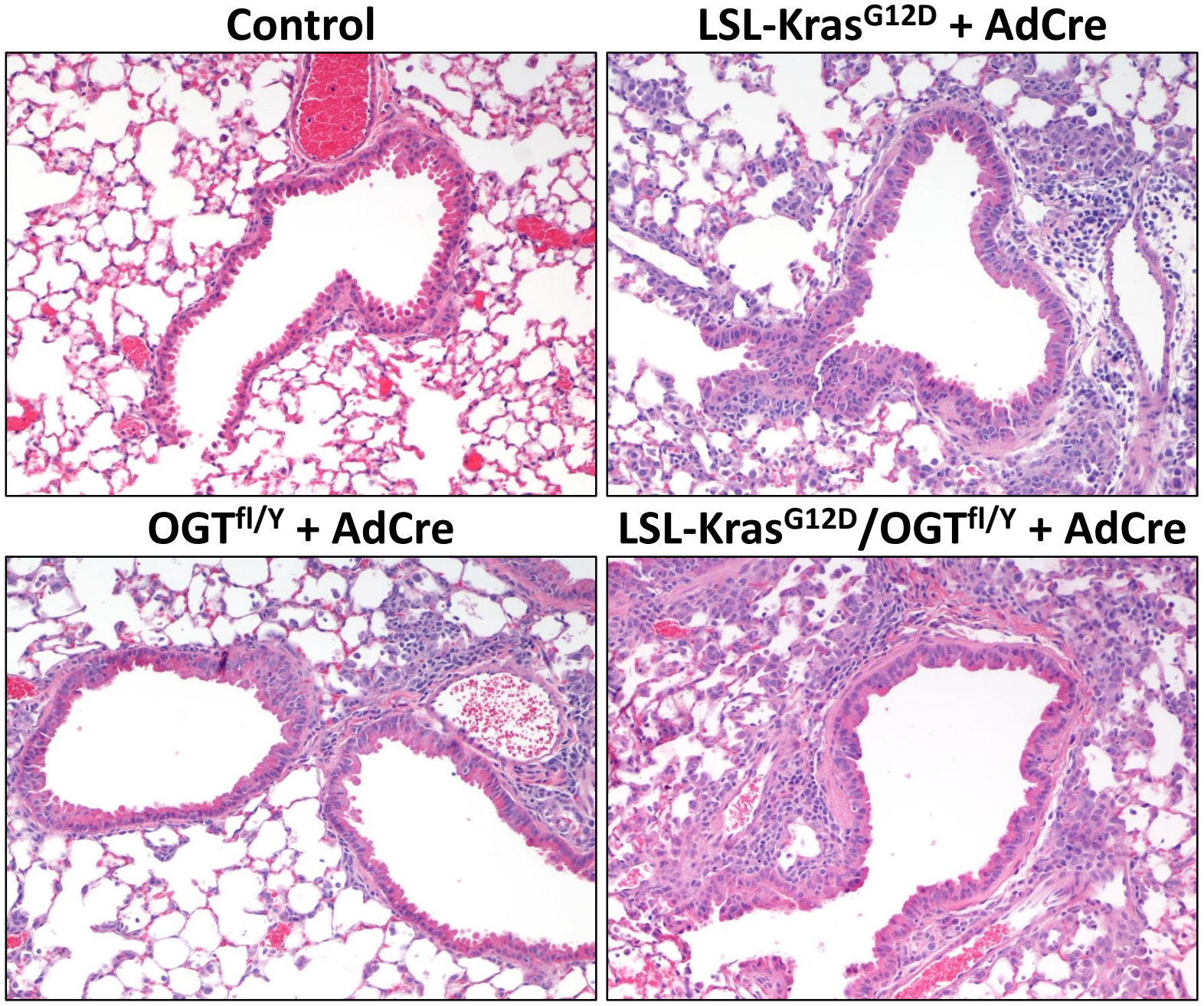
Control
LSL-Kras^{G12D} + AdCre
OGT$^{fl/Y}$ + AdCre
LSL-Kras^{G12D}/OGT$^{fl/Y}$ + AdCre

Fig. s11. Morphology of LSL-Kras^{G12D}/OGT$^{fl/Y}$ mouse lung tissue 8 days after AdCre. No relative increased cell death was observed in the lung tissue of OGT knockout mice either with or without concomitant activation of *Kras^{G12D}*. LSL-Kras^{G12D} (LSL) and LSL-Kras^{G12D}/OGT$^{fl/Y}$ (LSL-OGT$^{-/Y}$) mouse lungs demonstrated early atypical hyperplasia, but there was not an obvious difference at this early time point. Adenoviral-Cre intranasal infection demonstrated general signs of inflammation equally across the mouse strains.

Fig s12

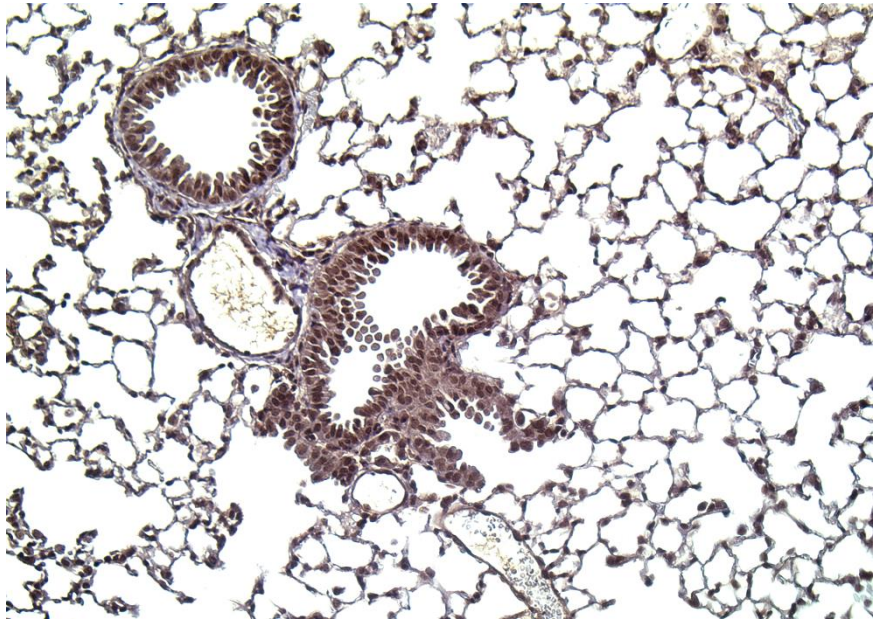

No AdCre
LSL

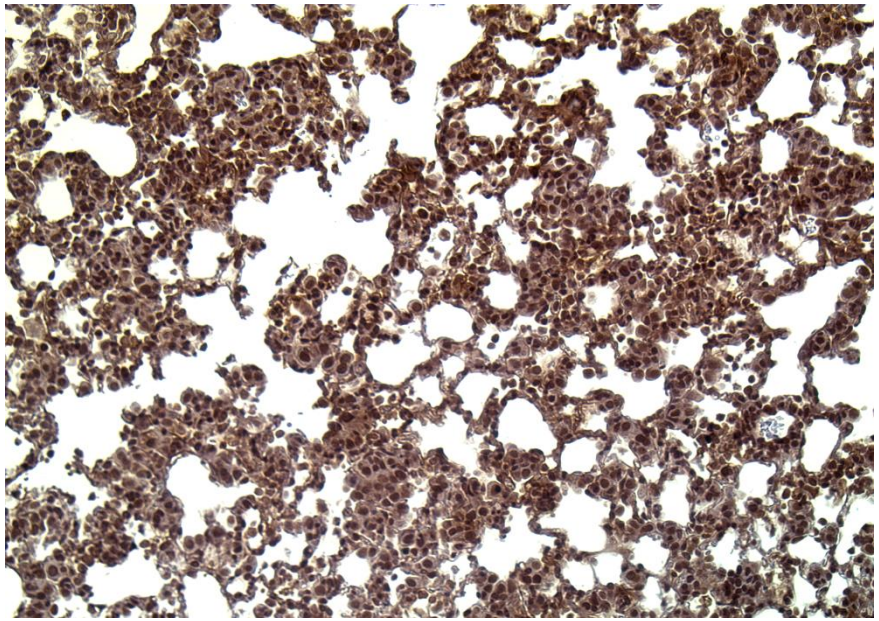

+ AdCre
LSL+TMG

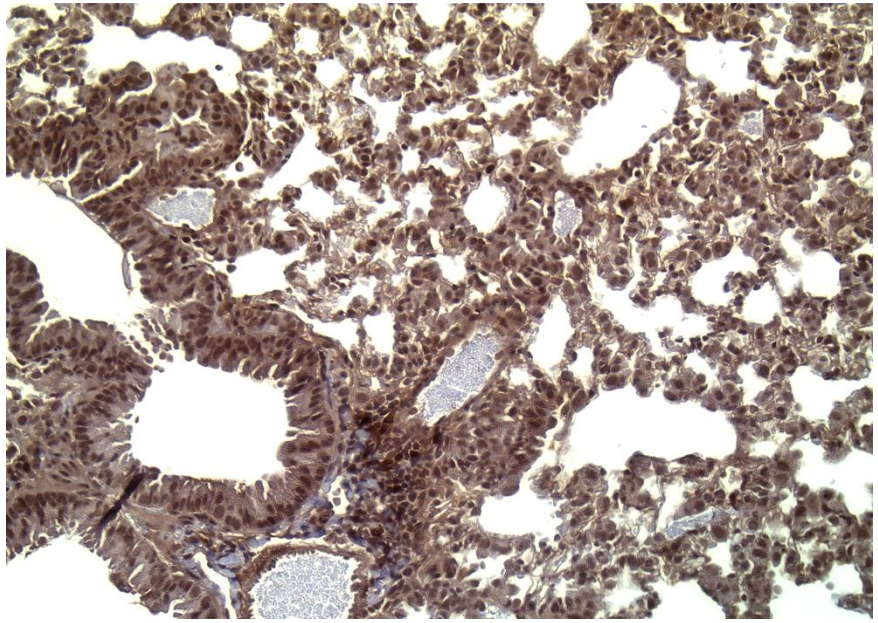

+ AdCre
LSL

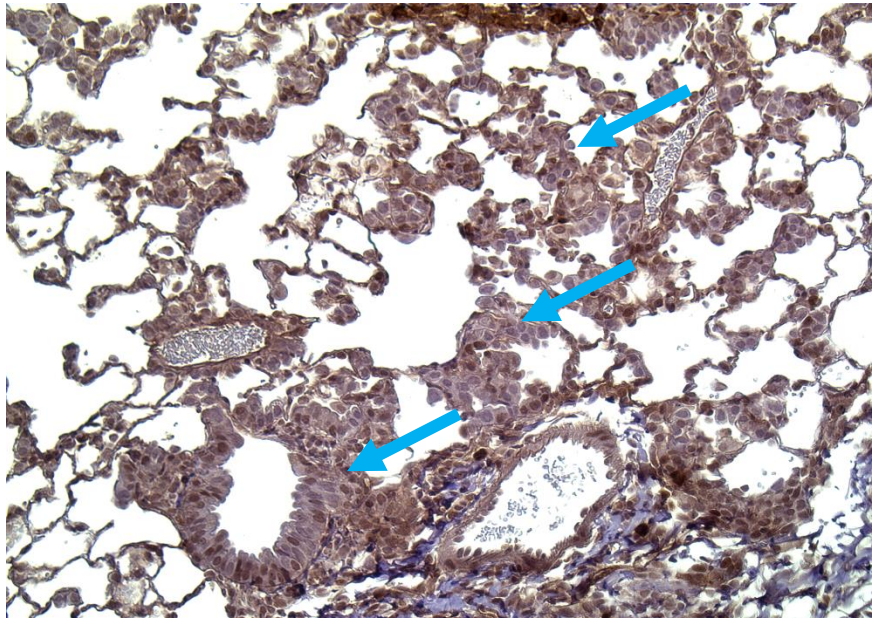

+ AdCre
LSL +OGT KO

Fig. s12. O-GlcNAc staining of LSL-Kras^{G12D}/OGT$^{fl/Y}$ mouse lung tissue 8 days after AdCre.
Blue arrows indicate cells with low or no O-GlcNAc staining. Original Magnificaiton: x200

Fig s13

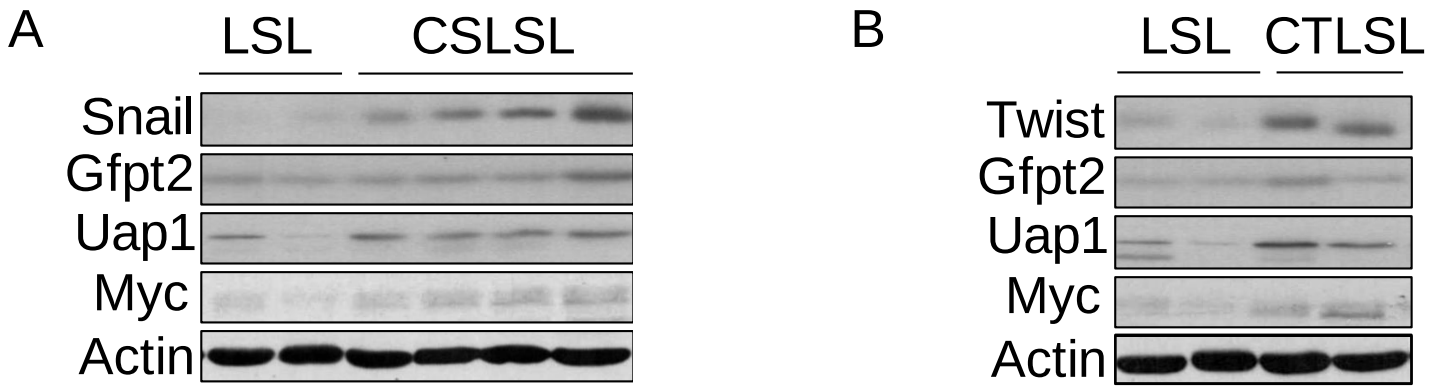
A
LSL
CSLSL
Snail
Gfpt2
Uap1
Myc
Actin
B
LSL
CTLSL
Twist
Gfpt2
Uap1
Myc
Actin

Fig. s13. The HBP and Myc in novel EMT mouse models of lung cancer. A-B, LSL mouse tumors were compared to CS-LSL (**A**) and CT-LSL (**B**) mouse tumors for HBP enzymes Gftp2 and Uap1, Myc, and SNAI1/TWIST by Western blot.